OH-Functionalized N-Doped Graphene Quantum Dots as an Efficient Metal-Free Catalysts for Oxygen Reduction Reaction in PEMFCs

Thangaraj Thiruppathiraja
Bharathiar University
Senthilkumar Lakshmipathi
lsenthilkumar@buc.edu.in
Bharathiar University

Research Article

Keywords: Oxygen Reduction Reaction, N-doped Graphene Quantum Dots, OH- Functionalization, Metal-Free Catalyst, Density Functional Theory

Posted Date: February 12th, 2024

DOI: https://doi.org/10.21203/rs.3.rs-3933196/v1

Additional Declarations: No competing interests reported.

Version of Record: A version of this preprint was published at Electrocatalysis on April 9th, 2024. See the published version at https://doi.org/10.1007/s12678-024-00869-8.

Abstract

Utilizing the density functional theory (DFT) method, we investigated the catalytic activity of N-doped graphene quantum dots (NGQDs) with nitrogen (N) atoms strategically doped at various active sites on the surface. We focused on exploring their efficiency in the $2e^-$ and $4e^-$ reduction pathways for oxygen reduction reaction (ORR). By introducing N-doping at the central benzene ring of carbon-based materials, we observed the formation of localized π-orbitals, significantly enhancing their electrocatalytic activity. In comparison to other reported catalysts, our N-doped GQDs metal-free electrocatalyst displayed remarkable adsorption capability. Furthermore, we introduced the hydroxyl group (OH) into the functionalized N-doped GQDs, which further improved electrocatalytic performance. This enhancement was attributed to the decreased HOMO-LUMO energy gap and increased chemical reactivity. The calculated free energy (ΔG) values for each elementary reaction step in the $4e^-$ reduction pathway were highly favorable and indicated the feasibility of the process. Our findings indicate that N-doped GQDs exhibit exceptional activity for the ORR, positioning them as promising carbon-based metal-free electrocatalysts. Consequently, they hold significant potential as an alternative to noble metal-based catalysts in proton exchange membrane fuel cells (PEMFC) and metal-air batteries.

Introduction

The PEMFC is an electrochemical energy conversion device that efficiently converts chemical energy into electrical energy while generating heat and water as byproducts [1, 2] [3]. PEMFCs have garnered significant attention as promising and sustainable clean energy solutions due to their notable advantages, including high conversion efficiency, environmental friendliness, and reliability [4, 5]. The PEMFC consists of two crucial electrodes: the anode, where the hydrogen oxidation reaction (HOR) occurs, and the oxygen reduction reaction (ORR) in the cathode. ORR, being the rate-limiting process in fuel cells, can follow two reaction pathways: the two-electron ($2e^-$) and four-electron ($4e^-$) pathways [6, 7]. For fuel cell applications, the $4e^-$ proton/electron transfer process in the ORR is preferred since it directly converts oxygen molecules (O_2) into water molecules (H_2O), offering superior conversion efficiency [8, 9]. However, the ORR process at the cathode is inherently slow, posing a significant challenge for fuel cell technology [10]. Although platinum (Pt) or Pt-based alloys are commonly used catalysts to expedite the reaction and are highly efficient [11, 12], their high cost hinders large-scale commercial applications [7, 13, 14]. Consequently, researchers are actively exploring non-precious metal catalysts (NPMCs) with excellent electrocatalytic performance for the ORR process [15, 16]. Nitrogen-doped (N-doped) carbon materials, including graphene (Gra), graphene quantum dots (GQDs), and carbon nanotubes (CNTs), have emerged as efficient metal-free electrocatalysts with high conversion efficiency when utilizing low-cost and abundant materials [17–23]. Therefore, developing NPMCs exhibiting impressive electrocatalytic performance for the ORR process is crucial for promoting fuel cell advancements [1, 24–28].

Recent studies have identified metal-free catalysts, such as N-doped GQDs, that exhibit promising electrocatalytic activity [23, 29–37]. GQDs possess several advantages as catalysts, including a high surface area-to-volume ratio, providing numerous active sites for catalytic reactions. Additionally, GQDs possess a high electron density and contain multiple edge sites, augmenting their catalytic activity. Moreover, GQDs display tunable energy levels attributable to the quantum confinement effect, making them appealing for various chemical reactions. The surface chemistry of GQDs can be modified by introducing different functional groups, such as carboxyl, amino, or hydroxyl groups, which further enhance their catalytic activity [38]. This study focuses on N-doping and OH functionalization of GQDs to improve their catalytic activity for ORR applications, employing state-of-the-art density functional theory (DFT). Furthermore, we systematically investigate the effects of OH-functionalized N-doped GQDs (OH-NGQDs) on thermochemical properties such as energy barriers (E_b), reaction energies (E_r), free energies (ΔG), adsorption strengths of intermediate ORR species, and overpotential values. The theoretical findings demonstrate that OH-functionalized N-doped graphene quantum dots (OH-NGQDs) are highly effective metal-free catalysts, facilitating the oxygen reduction reaction (ORR) process.

Computational details

The molecular formula of GQDs is $C_{24}H_{12,}$ and to create N-doped GQDs ($C_{23}NH_{12}$ (NGQDs)), the N-atom replaces a carbon (C) atom at the central benzene ring of the graphene structure. Functionalizing the edge site with OH results in an OH-NGQDs surface. The N-doping and OH functionalization significantly enhance the catalytic properties of GQDs [25].

All the geometry optimization of the molecular species, such as the reactants (R), intermediates (I), transition states (TS), and the final product (P) in the oxygen reduction reaction (ORR) mechanism using density functional theory (DFT) for all the reaction steps of the ORR mechanism with hybrid functional B3LYP [39] along with the 6-31G** [40] basis set is employed. All the R, I, and P geometries have only real frequencies, whereas the TS has only one imaginary frequency, which is the optimized geometry using the Berny algorithm. Furthermore, to verify whether the identified TS connects the designated R and P, intrinsic reaction coordinate (IRC) calculations for all R and P were performed at the same level of theory. All electronic structure calculations are done by Gaussian09 software [41].

Results and Discussion

Figure 1 depicts the relaxed structures of three different types of graphene quantum dots (GQDs): pure GQDs, N-doped GQDs (NGQDs), and OH-functionalized N-doped GQDs (OH-NGQDs). The pure GQDs structure consists of seven benzene rings comprising 24 carbon (C) atoms, with hydrogen (H) atoms passivated at the edge sites. The C-C bond length of 1.43 Å, while the C = C and C-H bond lengths are 1.43 Å and 1.09 Å. Upon replacing the C-atom with N-atom in NGQDs, the C-N bond length undergoes a variation within the range of 1.41 Å [42–44].

The OH-NGQDs, with the molecular formula $C_{23}N(OH)_{12}$, adopt a flat and planar structure consisting of seven interconnected benzene rings. The supplementary information (**Figure S1**) illustrates the structure of OH-NGQDs in various configurations with different positions for the N-atom. The quaternary position exhibits a negative frequency among these configurations, indicating its instability. Additionally, the edge OH-position disrupts the OH group, rendering it unsuitable for the oxygen reduction reaction (ORR) process. Consequently, the structure with N-atom positioned at the center is found to be the most stable configuration.

The formation energy (E_{form}) is calculated using the following equations [45, 46]:

$E_{form} = E_{NGQDs} + E_C - (E_{GQDs} + \mu_N)$ (1)

where E_{NGQDs} and E_{GQDs} indicate the total energies of NGQDs and the without N-doped GQDs, respectively. E_C and μ_N refer to the energy of the single C-atom in the GQDs and the chemical potential of a single N-atom in the N_2 molecule. The energy required for the NGQDs value is 0.59 eV and the E_{form} indicates an energetically favorable structure. This suggests that NGQDs is energetically feasible from the research viewpoint.

Frontier Molecular Orbitals

Frontier molecular orbital (FMO) energies of the highest occupied molecular orbital (E_{HOMO}), lowest unoccupied molecular orbital (E_{LUMO}) and HOMO-LUMO energy gap (E_{H-L}) [47, 48] for OH-NGQDs. The energy gap value of removing and adding an electron in a surface can be determined by ionization potential (IP) and electron affinity (EA). Furthermore, the IP is directly related to the HOMO energy value as $IP = -E_{HOMO,}$ and the EA can be estimated from the LUMO energy value as $EA = -E_{LUMO}$. The IP and EA values are important in examining the electrochemical reactivity of the considered systems. Furthermore, the chemical hardness (η) was calculated ($\eta = IP - EA/2$) using Koopman's theorem as depicted in Table 1.

Table 1
The HOMO (E_{HOMO}) and LUMO (E_{LUMO}) energy, HOMO-LUMO energy gap (E_{H-L}), ionization potential (IP), electron affinity (EA), and chemical hardness (η) for the GQDs, NGQDs and OH-NGQDs catalysts /eV.

Structure	E_{HOMO}	E_{LUMO}	E_{H-L}	IP	EA	η
GQDs	-5.46	-1.42	4.04	5.46	1.42	2.02
NGQDs	-3.08	-1.41	1.67	3.08	1.41	0.84
OH-NGQDs	-2.70	-1.06	1.65	2.70	1.06	0.82

The E_{H-L} gap for pure GQDs is 4.04 eV in good agreement with the similar geometry of GQDs (4.43 eV) [49] whereas in the case of NGQDs and OH-NGQDs, the E_{H-L} gap values are 1.67 and 1.65 eV. Therefore, the OH-NGQD catalyst has a small E_{H-L} gap, suggesting the higher reactivity of the system. The lower

chemical hardness value for OH-NGQDs shows that OH-functionalization significantly increases the chemical reactivity of the system [50]. Based on the other catalyst, the OH-NGQDs catalyst moved only further studies due to the reactivity parameters.

Hydroxyl group Functionalized N-doped GQDs

The Supplementary Information includes optimized structures for the metal-free catalyst OH-NGQDs in the presence of various ORR species, including *OO, *O + *O, *O + *OH, *OH + *OH, *H_2O_2, *OOH, *O, *OH and H_2O (*denoting the adsorbed on the catalyst). The structures are provided for the reactants (R), transition states (TS), intermediates (I), and the final product (P). These optimized structures are presented in **Figure S2** to **S6**. The reaction scheme illustrating the computed reaction mechanisms can be found in Fig. 2.

Table 2
Thermochemical properties of the OH-NGQDs catalyst for the ORR process using the B3LYP level of theory /eV.

Structure	Four electron reduction pathway					
	Associative Mechanism - Path 1			Dissociative Mechanism		
	ΔE	ΔH	ΔG	ΔE	ΔH	ΔG
R1	0	0	0	0	0	0
TS1	a	a	a	0.23	0.14	0.40
I1	-0.06	-0.07	-0.04	0.18	0.11	0.34
R2	0	0	0	0	0	0
TS2	1.29	1.29	1.29	1.15	1.15	1.15
I2	-0.99	-0.96	-1.03	-1.37	-1.35	-1.39
R3	0	0	0	0	0	0
TS3	0.74	0.76	0.72	1.40	1.41	1.40
I3	-1.09	-1.05	-1.16	-0.25	-0.20	-0.34
R4	0	0	0	0	0	0
TS4	0.64	0.63	0.65	0.64	0.63	0.65
I4	-1.22	-1.21	-1.21	-1.22	-1.21	-1.21
R5	0	0	0	0	0	0
TS5	0.97	0.98	0.95	0.97	0.98	0.95
P1	-1.36	-1.26	-1.52	-1.36	-1.26	-1.52

(a) Indicates could not locate the TS

Thermochemical parameters for both the proposed 4e$^-$ reduction pathway involving the associative mechanism (path-1-2-3) and the dissociative mechanism, as well as the 2e$^-$ reduction pathway on the OH-NGQDs catalyst have been determined. **Table S1** and **S2** present the obtained results. It is observed that the free energy limit is higher for the associative mechanism path-2-3, indicating that this pathway is less favorable. Furthermore, the 2e$^-$ reduction pathway results suggest that the ORR reaction process is not applicable to the OH-NGQDs catalyst. As a result, the most favorable pathways for the ORR process on the OH-NGQDs catalyst are the associative mechanism path-1 and the dissociative mechanism are given in Table 2. Consequently, only these reaction pathways were investigated in this study. The relative energy profile of the ORR steps is depicted in **Figure S7** and the validity of each elementary reaction step is confirmed through the intrinsic reaction coordinate (IRC) as shown in **Figure S8** (the graph displays the *OOH and *O + *OH species).

Four Electron Reduction Pathway

The reaction mechanism for the $4e^-$ reduction pathway in the OH-NGQDs catalyst can be described as follows. Two possible reaction steps are observed upon the adsorption of an oxygen molecule (O_2). The first reaction step follows an associative mechanism [51, 52], while the second reaction step proceeds via a dissociative mechanism [33, 53]. In the associative mechanism, each elementary reaction step is sequentially followed.

Associative Mechanism Path-1 (AMP-1)

The initial step involves the adsorption of the O_2 molecule on various positions of the OH-NGQDs catalyst for the ORR process (as shown in **Figure S9**). Subsequently, a more stable configuration is identified. The first reaction step (R1) involves the interaction of the O_2 molecule with the central benzene ring C-atom near the doped N-atom. The bond length of O_2 molecule (O-O) is elongated by 1.25 Å with the catalyst compared to 1.22 Å without the catalyst. This elongation allows for easy diffusion of the O_2 molecule, making it favorable for the ORR mechanism. The reaction energy (ΔE) is slightly exothermic. In the intermediate step (I1), the free energy (ΔG) for the OH-NGQDs catalyst is equal to that of mono-Co-PPy (-0.03 eV) [54], indicating that the reactions are spontaneous. Therefore, the oxygenation process is energetically favorable and feasible on the OH-NGQDs catalyst.

The addition of hydrogen (H) to the adsorbed $*O_2$ molecule on the OH-NGQDs catalyst results in the formation of *OOH molecule after relaxation. In this step, TS2 is identified with an energy barrier of 1.29 eV on the OH-NGQDs surface which is lower than that of PYRI-SUMA (1.42 eV) [34]. The reaction energy of the OH-NGQDs catalyst is highly exothermic compared to Sn-Gra (-0.69 eV) [55], FePc (-0.95 eV) [56], and RhN_2-GN (-0.74 eV) [51]. In intermediate step I2, the reaction is spontaneous as ΔG is negative (-1.03 eV) compared to Co-PPy (-0.46 eV) [54], Fe-$C_{24}N_{24}$ (-0.36 eV) [27], and CN-Sheet (-1.02 eV) [57]. The second H-atom interacts with the *OOH molecule adsorbed on the OH-NGQDs catalyst, forming the first water (H_2O) molecule. The minimum energy barrier of TS3 on the OH-NGQDs catalyst (0.74 eV) is lower than that of P-Gra (0.86 eV) [58]. The ΔE is highly exothermic (-1.09 eV) compared to Pt(111) (-0.14 eV) [52] and Pt/Ni (-0.60 eV) [52]. In intermediate step I3, the ΔG value is highly negative for the formation of the first H_2O molecule compared to CoO(100) (-0.60 eV) [59]. Thus, the formation of the H_2O molecule is energetically more favorable on the OH-NGQDs catalyst.

Next, the hydrogenation of the *O atom adsorbed on the OH-NGQDs catalyst leads to the formation of *OH molecule. The minimum energy barrier of TS4 is 0.64 eV due to the strong interaction of *OH with the C-atom near the N-atom, in comparison to Pt(111) (0.79 eV) [52], RhN_2-GN (1.08 eV) [51], and FeN_2-Gra (1.08 eV) [60]. The ΔE of the OH-NGQDs surface is more exothermic than that of Pt(111) (-0.14 eV) [52], Pt/Ni (-0.66 eV) [52], and FePc (-0.66 eV) [56]. In intermediate step I4, the ΔG value is more negative for the OH-NGQDs catalyst compared to $C_{23}H_{12}N$ (-1.06 eV) [61], Fe-$C_{24}N_{24}$ (-0.89 eV) [27], and Co-PPy (-1.18 eV) [54], indicating that this reaction is feasible and energetically favorable. The final step involves

the interaction of the H-atom with the OH-NGQDs catalyst, forming a second H_2O molecule. The energy barrier of TS5 (0.97 eV) is lower than that of SiC-1 (1.05 eV) [62], and the product H_2O molecule weakly interacts with the C-atom near the hydroxyl group (2.73 Å) [63]. ΔE is highly exothermic for the OH-NGQDs surface compared to BGNR (-1.23 eV) [64], Pt(111) (-0.70 eV) [52], and FePc (-0.57 eV) [56]. In the final product step (P1), ΔG is more negative for the OH-NGQDs surface than for $C_{23}H_{12}N$ (-0.44 eV) [61], CN sheet (-0.32 eV) [57], Fe-$C_{24}N_{24}$ (-0.73 eV) [27], and Co-PPy (-0.68 eV) [54]. These results demonstrate that the formation of the second H_2O molecule is more feasible and energetically favorable on the OH-NGQDs catalyst.

Dissociative Mechanism

The dissociation of the adsorbed O_2 molecule on the OH-NGQDs catalyst has also been considered. In the initial reactant step (R1), the O_2 molecule interacts with the C-atom near the N-atom of the OH-NGQDs surface, resulting in a C-O bond length of 3.08 Å. The TS1 exhibits a minimum energy barrier for the OH-NGQDs catalyst (0.23 eV) compared to SiC-1 (0.29 eV) [62] due to the strong interaction between the O-atom and the C-atom near the OH group. The intermediate (I1) involves splitting *O + *O atoms bonded with the C-atoms adsorbed on the OH-NGQDs catalyst with bond lengths of 1.36 and 1.43 Å. The initial reaction of O2 dissociation is endothermic with ΔE of 0.18 eV, similar to the result reported for CoO(111) (0.32 eV) [59], indicating that the initial reaction is energetically unfavorable.

The hydrogenation of the adsorbed *O + *O atom leads to the formation of *O + *OH. In the reactant step (R2), the *O + *O atom interacts with the C-atoms with bond lengths of 1.43 and 1.45 Å (C-O), and the H-atom adds to the adsorbed C-atom of the OH-NGQDs catalyst with a bond length of 1.11 Å (C-H). The TS2 is identified with an energy barrier of 1.15 eV. In the intermediate step (I2), the H-atom forms a bond with the adsorbed O-atom, resulting in the formation of *OH adsorbed on a C-atom with a bond length of 1.43 Å (C-O) while another O-atom interacts with the C-atom near the N-atom with a bond length of 1.44 Å (C-O). This reaction is exothermic with a ΔE of -1.37 eV equal to P-Gra (-1.37 eV) [58], indicating its energetic favorability.

Introducing a second H-atom into the OH-NGQDs catalyst occurs in the reactant step (R3). The adsorbed *OH (1.44 Å) and *O atoms (1.45 and 1.46 Å) interact with the C-atoms near the N-atom while the H-atom interacts with the C-atom of the OH-NGQDs catalyst (C-H) with a bond length of 1.11 Å. The energy barrier of TS3 for the system is 1.40 eV, suggesting that the OH-NGQDs catalyst has lower catalytic activity and limited potential applications. In the intermediate step (I3), the H-atom attached to *O + *OH leads to the formation of the first H_2O molecule, which interacts with the O-atom connected to the N-atom with a bond length of 1.82 Å, and the O-atom bonded with N-atom with a bond length of 1.40 Å. This reaction is exothermic with a ΔE of -0.25 eV. The last two reaction steps, *O to *OH and *OH to H_2O, follow the associative mechanism path-1 for the OH-NGQDs catalyst.

By comparing the energy barrier and reaction energy values of the OH-NGQDs catalyst to those of the other referenced catalysts, it is evident that OH-NGQDs exhibit efficient catalytic performance for the ORR

reaction. The relative free energy diagram for the OH-NGQDs catalyst is depicted in Fig. 3, providing a visual representation of the energy profile. Moreover, the free energy for the complete $4e^-$ reduction pathway (-4.92 eV) [60], the OH-NGQDs catalyst of AMP-1 (-4.92 eV), and the dissociative mechanism (-4.46 eV) indicating an enhanced catalytic activity of the OH-NGQDs surface. These findings further support the notion that OH-NGQDs are a highly effective catalyst for facilitating the ORR process. Overall, the results obtained for the OH-NGQDs catalyst demonstrate excellent catalytic activity, highlighting its potential as a promising candidate for promoting the ORR reaction.

Adsorption Energy

The adsorption energies of intermediates (*OO, *O + *O, *O + *OH, *OOH, *O, *OH) and the final product (H_2O) of the ORR process have been calculated [65] and are presented in Table 3. The results show that the adsorption of $*O_2$ molecules on AMP-1 and the adsorption of *O + *O atoms in the dissociative mechanism are well-anchored on the C-atom near the N-atom. The *O + *OH species are found to interact with the C-atom near the N-atom. In the case of *OOH interaction with the C-atom, the adsorption energy for AMP-1 is -0.79 eV. The first H_2O molecule adsorbs on the O-atoms while the *O atom forms a strong bond with the N-atom. The adsorption energy for *OH interaction with AMP-1, bonded to the C-atom near the N-atom, is -2.03 eV. Finally, the second H_2O molecule forms the final product on AMP-1 with adsorption energy on the C-atom neighboring the OH group.

A comparison of our adsorption energy results with previous reports [25, 58, 66] reveals enhanced adsorption for the $4e^-$ reduction pathway on AMP-1. The initial step, where $*O_2$ molecules strongly interact with the OH-NGQDs catalyst, shows a strong adsorption energy compared to other catalysts [25, 58, 66]. In the final step, H_2O is physisorbed on the OH-NGQD catalyst while the H_2O molecule is replaced by an O_2 molecule [21, 38]. On the basis of the above discussion, it can be concluded that the $4e^-$ reduction pathway on AMP-1 demonstrates promising potential for catalytic applications.

Table 3
The adsorption energy (E_{ads}) of the OH-NGQDs catalyst in the ORR process /eV.

Adsorbates	Adsorption Energy (E_{ads})			
	OH-NGQD (Our work)	Pt(111) [66]	$MgPc(OH)_{16}$ [25]	P-Gra [58]
$*O_2$	-1.89	-0.62	-0.75	-0.19
*O + *O	-1.64	#	#	-2.66
*O + *OH	-2.54	#	#	-4.19
*OOH	-0.79	-0.94	-0.69	-1.62
*O	-2.94	-4.30	-1.21	-4.17
*OH	-2.03	-2.21	-2.17	-3.34
H_2O	-0.05	-0.20	-0.69	-0.14

 # Denotes unavailability of data

Overpotential

The overpotential (η^{ORR}) is calculated to evaluate the ORR reaction process performance in the presence of an electrocatalyst to derive the minimum overpotential in the OH-NGQDs catalyst. The adsorption energy of the intermediate ORR species *O, *OH, and *OOH can be determined [67]. For the four proton/electron transfer reaction steps, the reaction free energy has the same magnitude at zero potential (U = 0 V), calculated as 4.92 eV/4 = 1.23 eV. Herein, this is equivalent to all the elementary reaction steps of free energy being zero at the equilibrium potential of 1.23 eV. Hence, the free energy of the ORR catalyst can be determined from the following equations.

$\Delta G_1 = \Delta G_{OOH}^{*} - 4.92$ eV (2)

$\Delta G_2 = \Delta G_{O}^{*} - \Delta G_{OOH}^{*}$ (3)

$\Delta G_3 = \Delta G_{OH}^{*} - \Delta G_{O}^{*}$ (4)

$\Delta G_4 = - \Delta G_{OH}^{*}$ (5)

The rate-determining step (RDS) is each elementary reaction with maximum free energy, while the onset potential is gained by the equation below:

$G^{ORR} = \max\{\Delta G_1, \Delta G_2, \Delta G_3, \Delta G_4\}$ (6)

$\eta^{ORR} = |G^{ORR}|/e + 1.23$ V (7)

According to **Table S3**, the rate-limiting step (RLS) in the OH-NGQDs catalyst is identified as the hydrogenation of OOH* to form the first H_2O molecule [67–69]. The ORR reaction process is exothermic, the negative value of free energies (ΔG1, ΔG2, ΔG3, ΔG4), a reaction favorable to ORR mechanism. The minimum overpotential for the ORR catalyst reaction process is the same for both the $4e^-$ reduction pathway (AMP-1) and the dissociative mechanism (DM) which is 0.70 V. The onset potential for the OH-NGQDs catalyst is lesser than N-doped GQDs (0.79–0.90 V) [68] and N-doped graphene oxide (0.80 V) [70]. These results suggest that the OH-NGQDs catalyst can be utilized as a metal-free electrocatalyst for the ORR reaction. Importantly, the N-atom doping at the central benzene ring on the OH-NGQDs surface exhibits extraordinary efficiency.

Conclusions

We have successfully investigated the catalytic behavior of the OH-NGQDs catalyst for the $4e^-$ oxygen reduction reaction using DFT calculations. The adsorbate species ($*O_2$, *O+*O, *O+*OH, *OOH, *O, *OH, and H_2O) interact with an N-atom and a nearby C-atom in the OH-NGQDs catalyst, leading to highly favorable thermochemical parameters for the ORR process. The lower positive formation energy of NGQDs is favorable for chemical synthesis. The lower chemical hardness of OH-NGQDs shows that OH-functionalization significantly increases the chemical reactivity of the surface. The OH-functionalization with N-doped GQDs demonstrates excellent catalytic activity with lower energy barriers and all reactions occur spontaneously. Additionally, the minimum overpotential results indicate that the OH-NGQDs catalyst is well-suited for the ORR process in proton exchange membrane fuel cells (PEMFCs). These findings provide strong support for the utilization and development of graphene quantum dots as novel metal-free electrocatalysts for fuel cell technologies.

Declarations

Supplementary Data

The thermochemical properties of the OH-NGQDs catalyst for ORR, the rate-limiting step, maximum free energy and overpotential are calculated, the structure of various probability of the minimum energy configuration (N-Position) for OH-NGQDs, the optimized structures of OH-NGQDs catalyst ($4e^-$ reduction pathway and $2e^-$ reduction pathway) with adsorbate species in initial state (R), transition states (TS), intermediates (I) and final state (P) phases and their corresponding bond lengths, the relative energy profile of ORR steps, the IRC plot of ORR reactions, the various conformer of initial step of the molecular oxygen for ORR process are given in the Supplementary Information.

Declaration of Interests

The authors declare that they have no known competing financial interests or personal relationships that could have appeared to influence the work reported in this paper.

Acknowledgments

Thangaraj Thiruppathiraja would like to thank the Department of Science and Technology, New Delhi, India, for providing financial support [DST-PURSE (II) Fellowship/2020/407].

Author Contribution Statement

Thangaraj Thiruppathiraja: Methodology, Software, Data curation, Formal analysis, Writing - original draft.

Senthilkumar Lakshmipathi: Methodology, Software, Data curation, Formal analysis, review & editing.

References

1. Seo, M.H., et al., Theoretical insight into highly durable iron phthalocyanine derived non-precious catalysts for oxygen reduction reactions. Journal of Materials Chemistry A, 2014. 2(46): p. 19707-19716.
2. Winter, M. and R.J. Brodd, What Are Batteries, Fuel Cells, and Supercapacitors? Chemical Reviews, 2004. 104(10): p. 4245-4270.
3. Qu, L., et al., Nitrogen-Doped Graphene as Efficient Metal-Free Electrocatalyst for Oxygen Reduction in Fuel Cells. ACS Nano, 2010. 4(3): p. 1321-1326.
4. Chowdhury, C. and A. Datta, Silicon-Doped Nitrogen-Coordinated Graphene as Electrocatalyst for Oxygen Reduction Reaction. The Journal of Physical Chemistry C, 2018. 122(48): p. 27233-27240.
5. Shao, M., et al., Recent Advances in Electrocatalysts for Oxygen Reduction Reaction. Chemical Reviews, 2016. 116(6): p. 3594-3657.
6. Liu, D., et al., Recent Advances on Nonprecious Metal Porous Carbon-based Electrocatalysts for Oxygen Reduction Reaction. ChemElectroChem, 2018. 5(14): p. 1775-1785.
7. Nie, Y., L. Li, and Z. Wei, Recent advancements in Pt and Pt-free catalysts for oxygen reduction reaction. Chemical Society Reviews, 2015. 44(8): p. 2168-2201.
8. Feng, L.-y., Y.-j. Liu, and J.-X. Zhao, Iron-embedded boron nitride nanosheet as a promising electrocatalyst for the oxygen reduction reaction (ORR): A density functional theory (DFT) study. Journal of Power Sources, 2015. 287.
9. Wei, Q., et al., Nitrogen-Doped Carbon Nanotube and Graphene Materials for Oxygen Reduction Reactions. Catalysts, 2015. 5: p. 1574-1602.
10. Kiani, M., et al., Facile synthesis of magnesium ferrite nanoparticles supported on nitrogen and sulfur codoped carbon black as an efficient electrocatalyst for oxygen reduction reaction. Journal of Nanoparticle Research, 2019. 21(5): p. 99.
11. Yang, Z., et al., Sulfur-Doped Graphene as an Efficient Metal-free Cathode Catalyst for Oxygen Reduction. ACS nano, 2011. 6: p. 205-11.

12. Chandran, P., A. Ghosh, and S. Ramaprabhu, High-performance Platinum-free oxygen reduction reaction and hydrogen oxidation reaction catalyst in polymer electrolyte membrane fuel cell. Scientific Reports, 2018. 8(1): p. 3591.
13. Xia, W., et al., Earth-Abundant Nanomaterials for Oxygen Reduction. Angewandte Chemie International Edition, 2016. 55(8): p. 2650-2676.
14. Li, F., et al., Atomic Mechanism of Electrocatalytically Active Co–N Complexes in Graphene Basal Plane for Oxygen Reduction Reaction. ACS Applied Materials & Interfaces, 2015. 7(49): p. 27405-27413.
15. Dai, L., et al., Metal-Free Catalysts for Oxygen Reduction Reaction. Chemical Reviews, 2015. 115(11): p. 4823-4892.
16. Liu, X. and L. Dai, Carbon-based metal-free catalysts. Nature Reviews Materials, 2016. 1(11): p. 16064.
17. Wang, Z., et al., Nitrogen-Promoted Self-Assembly of N-Doped Carbon Nanotubes and Their Intrinsic Catalysis for Oxygen Reduction in Fuel Cells. ACS Nano, 2011. 5(3): p. 1677-1684.
18. Ratso, S., et al., Highly active nitrogen-doped few-layer graphene/carbon nanotube composite electrocatalyst for oxygen reduction reaction in alkaline media. Carbon, 2014. 73: p. 361-370.
19. Higgins, D., et al., The application of graphene and its composites in oxygen reduction electrocatalysis: a perspective and review of recent progress. Energy & Environmental Science, 2016. 9(2): p. 357-390.
20. Reda, M., H.A. Hansen, and T. Vegge, DFT study of stabilization effects on N-doped graphene for ORR catalysis. Catalysis Today, 2018. 312: p. 118-125.
21. Kattel, S., P. Atanassov, and B. Kiefer, Density functional theory study of the oxygen reduction reaction mechanism in a BN codoped graphene electrocatalyst. Journal of Materials Chemistry A, 2014. 2(26): p. 10273-10279.
22. Ferre-Vilaplana, A. and E. Herrero, Why nitrogen favors oxygen reduction on graphitic materials. Sustainable Energy & Fuels, 2019. 3(9): p. 2391-2398.
23. Wei, Q., et al., Nitrogen-Doped Carbon Nanotube and Graphene Materials for Oxygen Reduction Reactions. Catalysts, 2015. 5(3).
24. Gao, Y., et al., Graphdiyne-Supported Single-Atom-Sized Fe Catalysts for the Oxygen Reduction Reaction: DFT Predictions and Experimental Validations. ACS Catalysis, 2018. 8(11): p. 10364-10374.
25. Thiruppathiraja, T., et al., H, OH and COOH functionalized magnesium phthalocyanine as a catalyst for oxygen reduction reaction (ORR) – A DFT study. International Journal of Hydrogen Energy, 2020. 45(15): p. 8540-8548.
26. Zhang, Z., et al., Systematic study of transition-metal (Fe, Co, Ni, Cu) phthalocyanines as electrocatalysts for oxygen reduction and their evaluation by DFT. RSC Advances, 2016. 6(71): p. 67049-67056.

27. Modak, B., K. Srinivasu, and S.K. Ghosh, Exploring metal decorated Porphyrin-like Porous Fullerene as catalyst for oxygen reduction reaction: A DFT study. International Journal of Hydrogen Energy, 2017. 42(4): p. 2278-2287.
28. Tan, H., et al., Sub50 nm Iron–Nitrogen-Doped Hollow Carbon Sphere-Encapsulated Iron Carbide Nanoparticles as Efficient Oxygen Reduction Catalysts. Advanced Science, 2018. 5(7): p. 1800120.
29. Fazio, G., L. Ferrighi, and C. Di Valentin, Boron-doped graphene as active electrocatalyst for oxygen reduction reaction at a fuel-cell cathode. Journal of Catalysis, 2014. 318: p. 203-210.
30. Zou, X., L. Wang, and B.I. Yakobson, Mechanisms of the oxygen reduction reaction on B- and/or N-doped carbon nanomaterials with curvature and edge effects. Nanoscale, 2018. 10(3): p. 1129-1134.
31. Panchakarla, L.S., et al., Synthesis, Structure, and Properties of Boron- and Nitrogen-Doped Graphene. Advanced Materials, 2009. 21(46): p. 4726-4730.
32. Van Tam, T., et al., Synthesis of B-doped graphene quantum dots as a metal-free electrocatalyst for the oxygen reduction reaction. Journal of Materials Chemistry A, 2017. 5(21): p. 10537-10543.
33. Zhang, J., Z. Wang, and Z. Zhu, A density functional theory study on oxygen reduction reaction on nitrogen-doped graphene. Journal of Molecular Modeling, 2013. 19(12): p. 5515-5521.
34. Thiruppathiraja, T., A.L. Arokiyanathan, and S. Lakshmipathi, Pyrrolic, pyridinic, and graphitic sumanene as metal-free catalyst for oxygen reduction reaction – A density functional theory study. Fuel Cells, 2021. 21(6): p. 490-501.
35. Liu, R., et al., Nitrogen-doped graphdiyne as a metal-free catalyst for high-performance oxygen reduction reactions. Nanoscale, 2014. 6(19): p. 11336-11343.
36. Zhang, C., et al., Synthesis of Phosphorus-Doped Graphene and its Multifunctional Applications for Oxygen Reduction Reaction and Lithium Ion Batteries. Advanced Materials, 2013. 25(35): p. 4932-4937.
37. Yang, Z., et al., Sulfur-Doped Graphene as an Efficient Metal-free Cathode Catalyst for Oxygen Reduction. ACS Nano, 2012. 6(1): p. 205-211.
38. Zhang, P., et al., Size effect of oxygen reduction reaction on nitrogen-doped graphene quantum dots. RSC Advances, 2018. 8(1): p. 531-536.
39. Becke, A.D., Density-functional thermochemistry. III. The role of exact exchange. The Journal of Chemical Physics, 1993. 98(7): p. 5648-5652.
40. Hariharan, P.C. and J.A. Pople, The influence of polarization functions on molecular orbital hydrogenation energies. Theoretica chimica acta, 1973. 28(3): p. 213-222.
41. Frisch, M.J., et al., Gaussian 09. 2009, Gaussian, Inc.: Wallingford, CT, USA.
42. Pham, T.V., et al., High Areal Capacitance of N-Doped Graphene Synthesized by Arc Discharge. Advanced Functional Materials, 2019. 29(48): p. 1905511.
43. Armaković, S., et al., Aromaticity, response, and nonlinear optical properties of sumanene modified with boron and nitrogen atoms. Journal of Molecular Modeling, 2014. 20(12): p. 2538.

44. Cheviri, M. and S. Lakshmipathi, Nitrogen-Doped Buckybowls as Potential Scaffold Material for Lithium-Sulfur Battery: A DFT Study. Electrocatalysis, 2021.
45. Manjunatha, J.G., et al., Sodium dodecyl sulfate modified carbon nanotubes paste electrode as a novel sensor for the simultaneous determination of dopamine, ascorbic acid, and uric acid. Comptes Rendus Chimie, 2014. 17(5): p. 465-476.
46. Liu, F., et al., Systematic exploration of N, C configurational effects on the ORR performance of Fe–N doped graphene catalysts based on DFT calculations. RSC Advances, 2019. 9(39): p. 22656-22667.
47. Hu, X., et al., Adsorption and Activation of O2 on Nitrogen-Doped Carbon Nanotubes. The Journal of Physical Chemistry C, 2010. 114(21): p. 9603-9607.
48. Zhang, L. and Z. Xia, Mechanisms of Oxygen Reduction Reaction on Nitrogen-Doped Graphene for Fuel Cells. The Journal of Physical Chemistry C, 2011. 115(22): p. 11170-11176.
49. Li, Y., et al., Electronic and Optical Properties of Edge-Functionalized Graphene Quantum Dots and the Underlying Mechanism. The Journal of Physical Chemistry C, 2015. 119(44): p. 24950-24957.
50. Sharma, V., et al., Role of functionalized graphene quantum dots in hydrogen evolution reaction: A density functional theory study. International Journal of Hydrogen Energy, 2022.
51. Meng, Y., et al., Rhodium and Nitrogen Codoped Graphene as a Bifunctional Electrocatalyst for the Oxygen Reduction Reaction and CO2 Reduction Reaction: Mechanism Insights. The Journal of Physical Chemistry C, 2019. 123(9): p. 5176-5187.
52. Duan, Z. and G. Wang, A first principles study of oxygen reduction reaction on a Pt(111) surface modified by a subsurface transition metal M (M = Ni, Co, or Fe). Physical Chemistry Chemical Physics, 2011. 13(45): p. 20178-20187.
53. Zhang, J., Z. Wang, and Z. Zhu, The inherent kinetic electrochemical reduction of oxygen into H2O on FeN4-carbon: A density functional theory study. Journal of Power Sources, 2014. 255: p. 65-69.
54. Chen, X., et al., Density Functional Theory Study of the Oxygen Reduction Reaction on a Cobalt–Polypyrrole Composite Catalyst. The Journal of Physical Chemistry C, 2012. 116(23): p. 12553-12558.
55. Sun, X., et al., The oxygen reduction reaction mechanism on Sn doped graphene as an electrocatalyst in fuel cells: A DFT study. RSC Adv., 2017. 7: p. 729-734.
56. Sun, S., N. Jiang, and D. Xia, Density Functional Theory Study of the Oxygen Reduction Reaction on Metalloporphyrins and Metallophthalocyanines. The Journal of Physical Chemistry C, 2011. 115(19): p. 9511-9517.
57. Zhao, J. and Z. Chen, Carbon-Doped Boron Nitride Nanosheet: An Efficient Metal-Free Electrocatalyst for the Oxygen Reduction Reaction. The Journal of Physical Chemistry C, 2015. 119(47): p. 26348-26354.
58. Bai, X., et al., Theoretical insights on the reaction pathways for oxygen reduction reaction on phosphorus doped graphene. Carbon, 2016. 105.

59. Qin, B., et al., A density functional theory study of the oxygen reduction reaction on the (111) and (100) surfaces of cobalt(II) oxide. Progress in Reaction Kinetics and Mechanism, 2019. 44(2): p. 122-131.
60. Yang, Y., et al., A density functional study on the oxygen reduction reaction mechanism on FeN2-doped graphene. New Journal of Chemistry, 2018. 42(9): p. 6873-6879.
61. Zhang, P., et al., Size effect of oxygen reduction reaction on nitrogen-doped graphene quantum dots. RSC Advances, 2018. 8: p. 531-536.
62. Zhang, P., et al., Layered SiC Sheets: A Potential Catalyst for Oxygen Reduction Reaction. Scientific Reports, 2014. 4(1): p. 3821.
63. Priya, M., L. Senthilkumar, and P. Kolandaivel, Hydrogen-bonded complexes of serotonin with methanol and ethanol: A DFT study. Structural Chemistry, 2014. 25.
64. Wang, L., et al., Potential Application of Novel Boron-Doped Graphene Nanoribbon as Oxygen Reduction Reaction Catalyst. The Journal of Physical Chemistry C, 2016. 120(31): p. 17427-17434.
65. Shin, D.Y., et al., Density functional theory–based design of a Pt-skinned PtNi catalyst for the oxygen reduction reaction in fuel cells. Applied Surface Science, 2021. 565: p. 150518.
66. Li, K., et al., The oxygen reduction reaction on Pt(111) and Pt(100) surfaces substituted by subsurface Cu: a theoretical perspective. Journal of Materials Chemistry A, 2015. 3(21): p. 11444-11452.
67. Ma, R., et al., A review of oxygen reduction mechanisms for metal-free carbon-based electrocatalysts. npj Computational Materials, 2019. 5(1): p. 78.
68. Saidi, W.A., Oxygen Reduction Electrocatalysis Using N-Doped Graphene Quantum-Dots. The Journal of Physical Chemistry Letters, 2013. 4(23): p. 4160-4165.
69. Li, M., et al., N-doped graphene as catalysts for oxygen reduction and oxygen evolution reactions: Theoretical considerations. Journal of Catalysis, 2014. 314: p. 66-72.
70. Chanda, D., et al., Investigation of electrocatalytic activity on a N-doped reduced graphene oxide surface for the oxygen reduction reaction in an alkaline medium. International Journal of Hydrogen Energy, 2018. 43(27): p. 12129-12139.

Figures

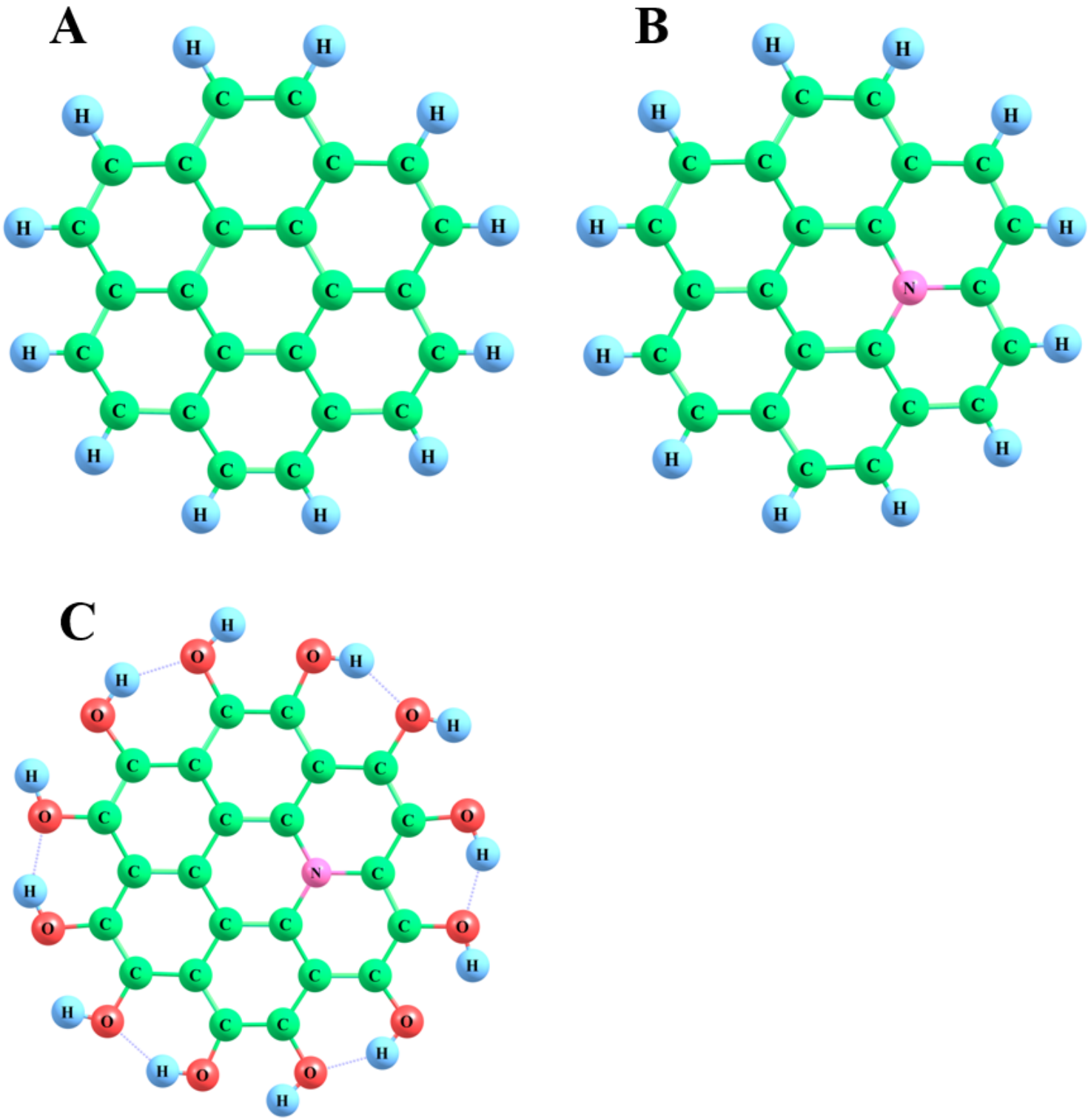

Figure 1

The optimized geometry of **A**) Graphene quantum dots (GQDs), **B**) N-doped graphene quantum dots (NGQDs), and **C**) Hydroxyl group functionalized N-doped graphene quantum dots (OH-NGQDs).

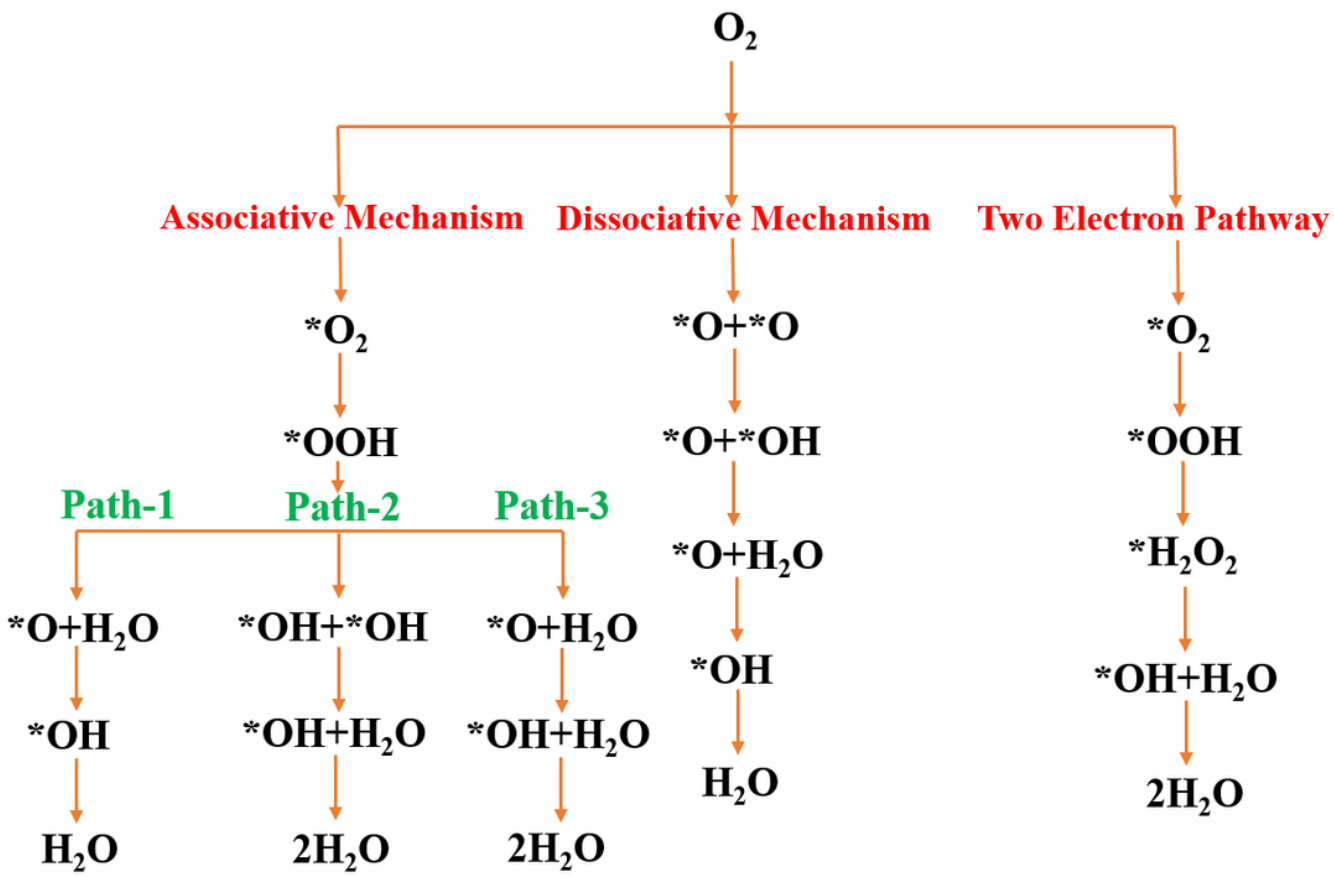

Figure 2

The overall reaction mechanism of the 4e$^-$ reduction pathway (associative mechanism path-1-2-3 and dissociative mechanism) and 2e$^-$ reduction pathway for ORR process.

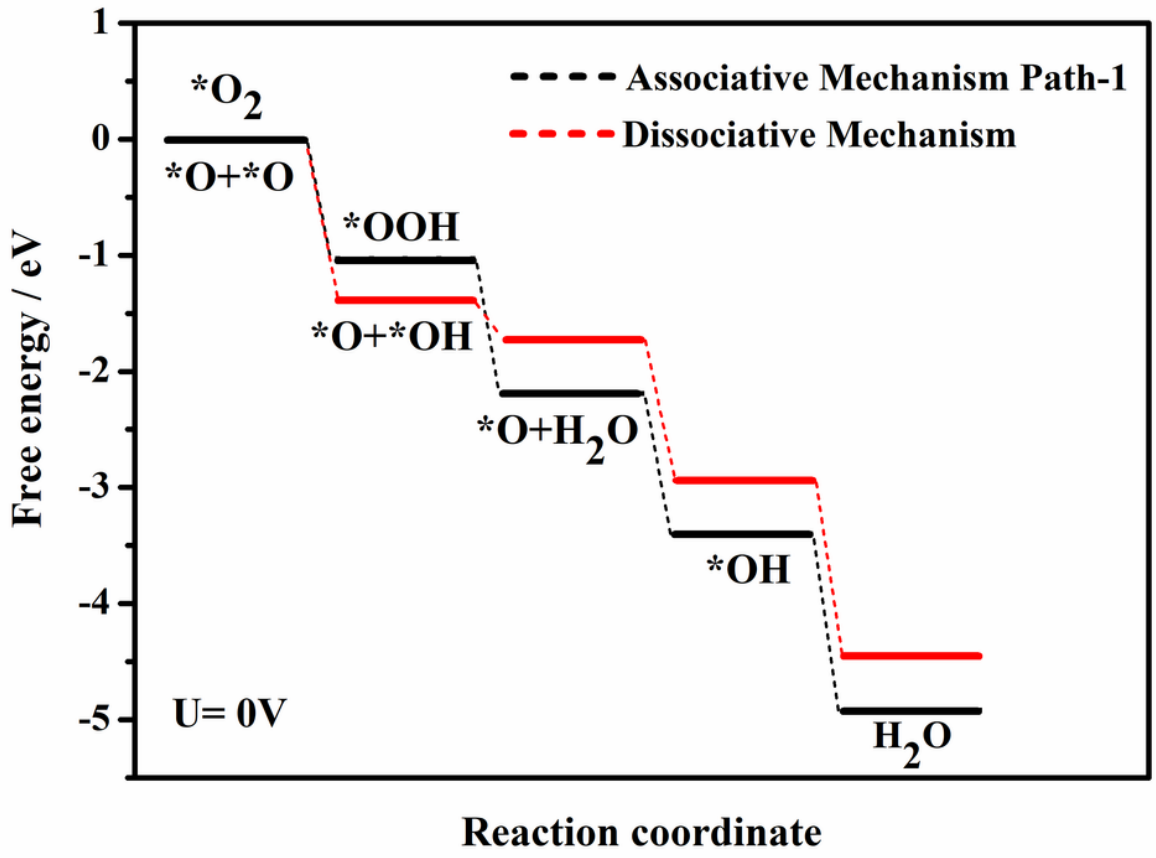

Figure 3

The free energy diagram for OH-NGQDs catalyst of the 4e$^-$ reduction pathway (associative mechanism path-1 and dissociative mechanism).

Supplementary Files

This is a list of supplementary files associated with this preprint. Click to download.

- SupplementaryInformation.doc